Int. J. Heat Mass Transfer. Vol. 30, No. 3, pp. 569–579, 1987
Printed in Great Britain

0017–9310/87 $3.00 + 0.00

Thermal interactions of a molten tin drop with water triggered by a low-pressure shock

S. H. HAN† and S. G. BANKOFF
Chemical Engineering Department, Northwestern University,
Evanston, IL 60201, U.S.A.

(*Received* 10 *June* 1985 *and in final form* 1 *July* 1986)

Abstract—Thermal interactions of a molten tin drop with water were studied with a dropping contact mode in a shock tube geometry. The interaction was triggered by collapsing the initial vapor/gas bubble with a low-pressure (< 0.8 MPa) shock. The hollow, porous, shell-like debris indicates that violent boiling, or homogeneous nucleation, of penetrated water, followed by turbulent mixing, might be a dominant mechanism for fragmentation of tin drops. An empirical correlation was obtained for the fragmentation time scale. The average heat transfer rate during the interaction was found to be in the range 1–10 kW. The conversion efficiency of thermal energy to mechanical energy of the water column above the tin drop was found to be in the range 0.1–1.0%.

1. INTRODUCTION

IN A SEVERE light-water reactor accident, molten fuel and steel could come into contact with the water in the lower plenum and undergo an explosive interaction, which might damage the reactor containment [1]. To provide the energy to escalate fuel–coolant interactions and sustain the pressure wave, fuel–coolant heat transfer is required immediately behind the front at rates which imply a large enhancement of heat transfer area. Two pressure-induced fragmentation mechanisms have been proposed: boiling fragmentation, and purely hydrodynamic fragmentation, which depends only on the relative velocity between fuel and coolant. Since detonation calculations with hydrodynamic fragmentation alone require a rather large escalation length for the development of full detonations [2], fragmentation mechanisms with shorter interaction lengths will be operative during the escalation stage and possibly longer. Generally, the mixing of fuel drops with a volatile coolant results in stable film boiling around the drops. Hence fragmentation mechanisms related to the boiling of the coolant, such as nucleate or transition boiling [3], penetration of a water jet [4], coolant entrapment [5], vapor blanket collapse [6], or turbulent mixing, have received considerable attention. These mechanisms are often non-exclusive, and more than one may be operative at the same time. In fact, cyclic processes have been observed in several experiments [6–8].

In the present work attention is focused on boiling fragmentation of fuel drops. To prevent hydrodynamic fragmentation of fuel drops, fuel–coolant interactions were triggered by generating a low-pressure (< 0.8 MPa) shock wave after a single drop of molten tin was dropped into a column of water within a vertical shock tube. Boiling fragmentation could thus be observed at initial pressures of 0.1–0.5 MPa. Most previous fragmentation experiments with tin and other materials have been performed at atmospheric pressure without external triggering. However, exploding wires, which generate a very sharp pressure pulse and following rarefaction wave, have also been used to trigger the interaction [9, 10]. In either case the fragmentation proceeds under different conditions than a vapor explosion, where the fragmentation proceeds behind the detonation shock front at essentially the shock pressure. This can strongly influence the fragmentation rate and the mechanical work output. Conducting the fragmentation study in a shock tube has the advantage that fragmentation takes place at the pressure behind the shock front. In addition, single-drop experiments, while they can be observed and modeled much more readily than multiple-drop experiments, have the disadvantage of excessive heat losses to the surrounding subcooled water and weaker mechanical constraints on the expanding mixture. The use of a liquid-column shock tube in which to conduct the interaction has the further advantage that the impulse imparted to the overlying liquid can be rather precisely calculated from the pressure traces, and the mechanical work performed can be deduced therefrom.

In this work the time constant for the fragmentation, the conversion efficiency of thermal energy to mechanical energy, and the heat transfer rate, as well as the fragmentation mechanism, were calculated, based on the pressure–time history and the high-speed photographs. In addition, the effects of parameters, such as ambient pressure, shock pressure, contact Weber number, water subcooling, and melt temperature, were also studied.

† Present Address: Korea Power Engineering Co., P. O. Box 109, Yeoeuido, Seoul, Korea.

NOMENCLATURE

A	area
C_p	specific heat
D	diameter
H	enthalpy
h	heat transfer coefficient
h_{sf}	heat of fusion
h_{fg}	heat of vaporization
k	thermal conductivity
Ja^+	thermal Jakob number
m	mass
P	pressure
P^*	peak pressure
ΔP	shock pressure
ΔP^+	dimensionless shock pressure
q	heat transfer rate
T	temperature
T^+	dimensionless breakup time
t	time
u	velocity
We	contact Weber number
We^+	thermal Weber number
X	vapor film thickness or crust thickness
X^*	minimum film thickness.

Greek symbols

α	thermal diffusivity
λ	crust growth constant
μ	viscosity
ξ	fractional heat loss to the surrounding water
ρ	density
σ	surface tension
τ	time constant.

Superscripts

b	breakup
c	characteristic
f	fuel or final
g	gas
l	liquid
m	melting
s	solid
sat	saturated
0	initial
∞	terminal.

2. EXPERIMENT

2.1. *Shock tube*

As shown in Fig. 1, the shock tube [11] consists of a driven section constructed of thin-walled 50 mm O.D. stainless steel tubing surmounted by a driver section. The thin mylar diaphragm between the two sections is ruptured by a plunger attached to a piston. This is actuated by a solenoid valve (MV1) with a pre-set time delay, in order to locate the tin drop near the top of the window when the pressure shock arrives. The piston cylinder is connected to the driver section via a check valve (CV1) to equalize pressures during pressurization of the driver section. The pressure in the driver section is controlled by a regulating valve (RV1) connected to a nitrogen gas cylinder, and is measured by a precision pressure gauge. Air is removed from the driven section by a vacuum pump protected by a trap, and is then replaced with nitrogen gas to prevent oxidation of tin. The initial system pressure is controlled by a regulating valve (RV2) for pressures above atmospheric. Pressure variations in the driven section are measured by two quartz pressure transducers (PT1, PT2), one in the water and the other in the overlying gas. A third pressure transducer (PT3) is placed 70 mm below the diaphragm to initiate data sampling by a microcomputer. The resonant frequency and the rise time of the pressure transducer are 250 kHz and 2 μs, respectively. A melting crucible made of stainless steel, 12 mm diameter × 20 mm, is supported by a 3 mm steel rod and heated by a high watt density (160 kW m^{-2}) electric heater of diameter 1.25 mm wound on the outside wall of the crucible. The molten tin is dropped into water by turning the rod. A light source and a photo-detector are placed 10 mm below the crucible. The light beam is broken by the falling tin drop, which then actuates the solenoid valve (MV1) with a pre-set time delay. The temperature of the molten tin in the crucible is measured by a thermocouple. The location of the fragmenting drop relative to PT2 is determined from the high-speed photographs.

2.2. *Experimental conditions*

Spontaneous interaction of tin and water at atmospheric pressure can be avoided in a certain range of tin and water temperatures. However, it appears that the spontaneous interaction zone is dependent upon the contact mode of fuel and coolant. In experiments by Dullforce *et al.* [12] 12 g of molten tin were dropped into water 3 cm below the tin crucible, while single water drops were released 5 cm above the molten tin surface in experiments by Wey *et al.* [7]. In addition, Reynolds *et al.* [13] found that the extent of the spontaneous interaction zone was slightly dependent on the mass of tin. Since molten tin drops were dropped into water in the present experiments, the conditions mentioned above can be reduced to a contact Weber number We^*, based on the drop velocity upon entering the water. In the Dullforce experiments the contact Weber number was approximately 13, which is very close to the critical value for Weber breakup [14].

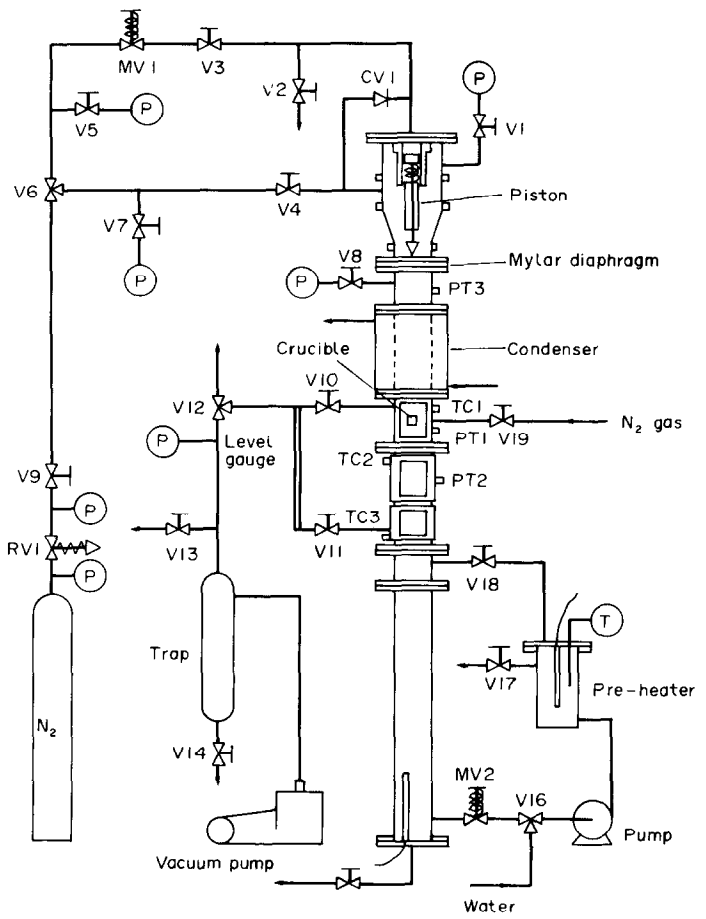

FIG. 1. Schematic description of the low-pressure shock tube.

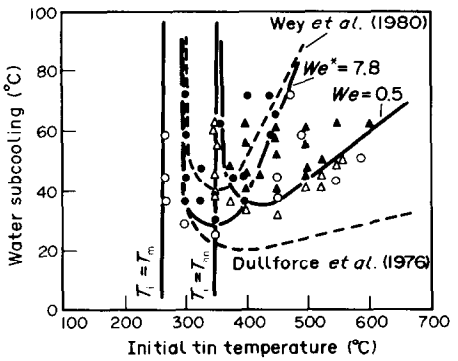

FIG. 2. Spontaneous temperature-interaction zone for tin and water as a function of the contact Weber number at atmospheric pressure.

Hence, a series of spontaneous interaction experiments was conducted to determine the spontaneous interaction zone for contact Weber numbers less than 13. Figure 2 shows the spontaneous temperature-interaction zone as a function of the contact Weber number at atmospheric pressure. It is seen that a shift of the spontaneous temperature-interaction zone occurs, depending on the contact Weber number. When $We^* = 7.8$, the temperature-interaction zone is close to the region found by Wey *et al.* [7]. This means the effect of air entrainment is not very significant. However, the reason for a shift of the interaction zone at $We^* = 0.5$ is not clear. A contact Weber number of 7.8 was chosen for the present experiments, owing to the limitation imposed by the high-watt-density heater. The maximum tin temperature which could be obtained from the heater was about 650°C. At pressures above 0.2 MPa, spontaneous interactions were completely suppressed for the same range of tin and water temperatures. The ambient pressure is thus an important parameter for fragmentation.

The pressure rise time constant may play an important role in the triggering of interactions. However, it was found by Sharon and Bankoff [8], in their fuel–coolant interaction experiments in a shock tube with initially-established film boiling, that the pressure time constant had no effect on the triggering of interactions when the time constant was less than 4 ms. Therefore, the pressure rise time constant was excluded from the experimental parameters.

The ranges of the experimental parameters were

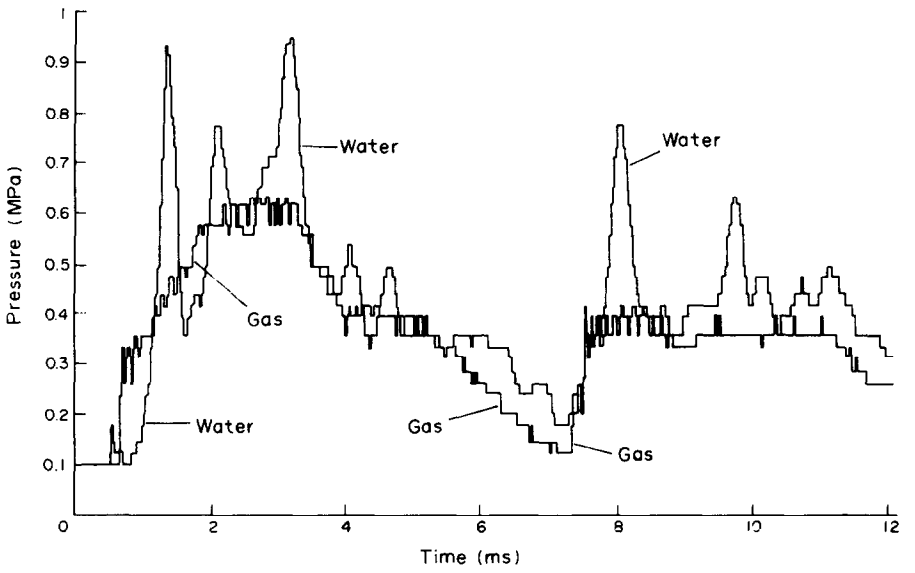

FIG. 3. Time history of pressures for strong interactions: $\Delta P = 0.54$ MPa, $P_0 = 0.1$ MPa, $T_f = 565°C$, $T_l = 66°C$.

thus determined as follows:

initial tin temperature	= 500–600 °C
initial water subcooling	= 10–60 °C
initial pressure	= 0.1–0.5 MPa
shock pressure	= 0.2–0.75 MPa
contact Weber number	= 7.8.

3. EXPERIMENTAL RESULTS

3.1. *Time history of pressures*

A representative time history of pressures in the water and in the gas phase above the water for strong interactions is shown in Fig. 3. The gas phase pressure shows the characteristics of the pressure shock generated, and the water pressure shows three strong peaks during the first 3 ms. Since the drop is initially in a film boiling mode, the first peak is believed to be due to the collapse of the initial vapor bubble, while the second and third peaks are associated with the collapse of the vapor bubbles generated during the interaction. This coincides with the observations from the high-speed photographs, which show three consecutive collapse and growth periods of the vapor/gas region during the first 3 ms. The water pressure remains a little below the gas phase pressure between the pressure peaks, as would be associated with the decelerating growth and accelerating collapse of a vapor bubble. The reflected wave causes additional interaction at about 8 ms. More details are given by Han [15].

3.2. *High-speed photographs*

Figure 4 shows a typical deformation of a tin drop behind a pressure shock for strong interactions. The drop is initially ellipsoidal, and seems to entrain noncondensable gas as it enters into the water. Since the tin drop cannot be clearly identified due to the presence of vapor during the deformation, only the boundaries of the interaction region are shown. It is seen that, since most of the entrained gas plus vapor was located near the top of the drop, cyclic bubble growth and collapse occurs only in this region. Water penetrates into the drop after the bubble is collapsed, resulting in the expansion of the lower boundary in all directions. During the expansion phase the boundary becomes very wavy. Some of the fragments are believed to be ejected from the interaction region, which is confirmed by the presence of very fine particles in the debris. Such a fragmentation mechanism may be explained by boiling of the penetrated water or by an impulsive motion of coolant and splash of fuel [16], or a combination of both. As shown in Fig. 4 (Frames 4–6), the penetration of water causes a local swell of the bottom surface of a tin drop. After the tenth frame no significant changes in the boundary are observed, and smooth boiling of the entrapped water inside the tin drop or surrounding water occurs after the tenth frame. The vapor/gas mixture eventually separates from the drop as it cools and rises. The elapsed time to the tenth frame is about 2.7 ms. For the mild interactions, a large vapor/gas bubble is always observed to be present at the top of the drop throughout the interactions, while the top boundary undergoes little expansion even after the initial bubble has ceased to collapse.

3.3. *Effect of the shock pressure*

Spontaneous interactions can be suppressed either at ambient pressures greater than 0.1 MPa or at high tin and water temperature conditions, even at atmospheric pressure. However, violent interactions can be initiated under these conditions if an external

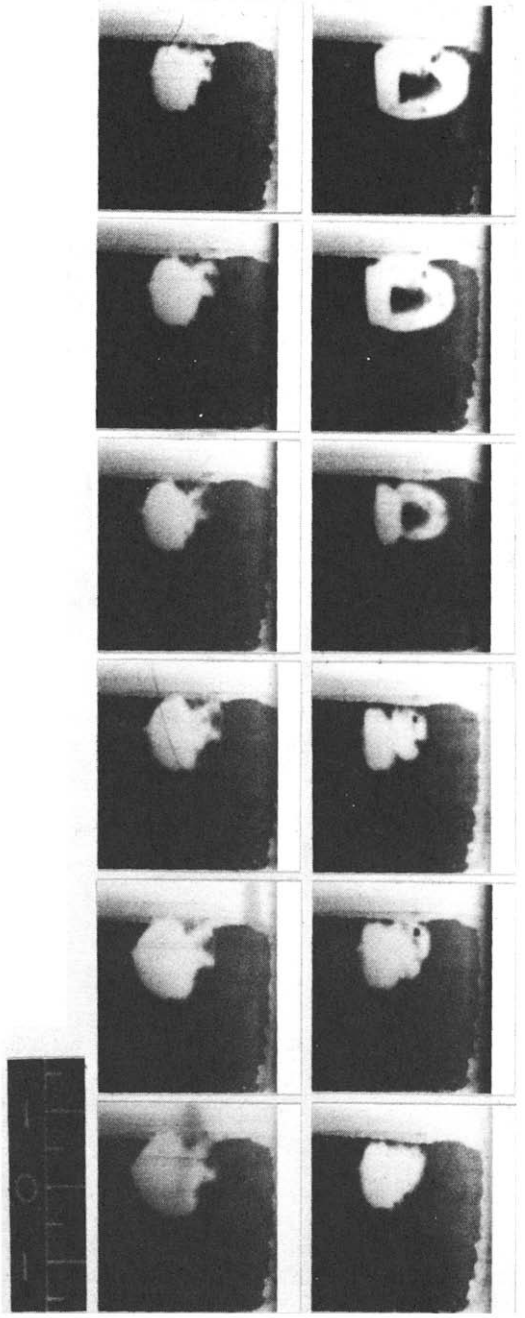

FIG. 4. Deformation of a tin drop for strong interactions: $\Delta P = 0.31$ MPa, $P_0 = 0.1$ MPa, $T_i = 78°C$, $T_f = 593°C$ (delay time = 120 ms, speed = 0.274 ms per frame).

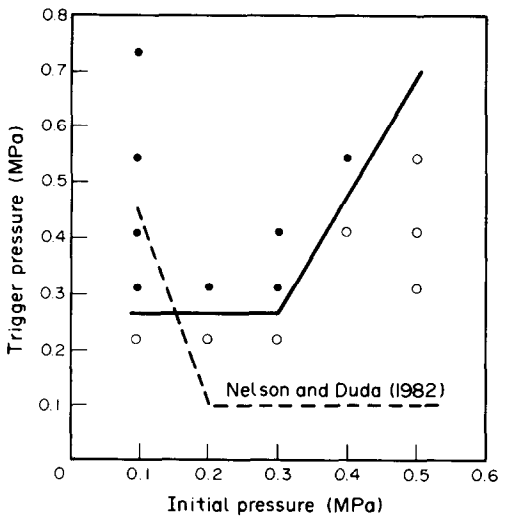

FIG. 5. Triggered pressure-interaction zone for tin and water: $T_i = 80°C$, $T_f = 550$–$570°C$.

trigger is applied. Figure 5 shows the shock pressures required for strong interactions at various initial pressures. The shock pressure is defined as the difference between the final pressure and the initial pressure, where the final pressure is the average water pressure measured near the drop during 1–3 ms after shock arrival. It is seen that a sudden increase in the shock pressure occurs for initial pressures greater than 0.3 MPa. However, a decrease in the required shock pressure as the initial pressure increases in the neighborhood of atmospheric pressure, observed by Nelson and Duda [17], was not found. In the Nelson and Duda experiments the initial temperature (2000 °C) of the molten iron oxide drops was about 1200 °C above the minimum film boiling temperature of water, so that the stability of the initial vapor film decreased as the initial pressure increased at constant water temperature, owing to the increase in the liquid subcooling, at initial pressures less than 0.2 MPa. On the other hand, the sharp increase observed by Nelson and Duda in the required pressure pulse above 0.8 MPa may be related to the increased vapor density, which inhibits complete collapse of the vapor film and also results in slower bubble growth. In the present experiment the initial tin temperature (550–560 °C) was only about 200 °C above the minimum film boiling temperature with 80 °C water, and the required shock strength was much less than with molten iron oxide. This may be related to the absence of a decrease in the required shock pressure as the initial pressure increases. Besides, the triggers were quite different, as noted above.

3.4. *Effects of initial pressure and water subcooling*

Figure 6 shows the triggered-interaction zone for various water temperatures and initial pressures. The shock pressure was kept constant at 0.41 MPa. The degree of water subcooling necessary for strong interactions rose sharply when the initial pressure was increased to 0.3 MPa. This may be interpreted in terms of the increased vapor density at high initial pressures. As the initial pressure increases at constant water subcooling, the higher vapor density inhibits complete collapse of the vapor film. Hence an initially less stable vapor film, which is obtainable at larger water subcoolings, is required in order to initiate strong interactions at the same shock pressure. Since the trigger mechanism is quite different, it is difficult to make a direct comparison of these results with the

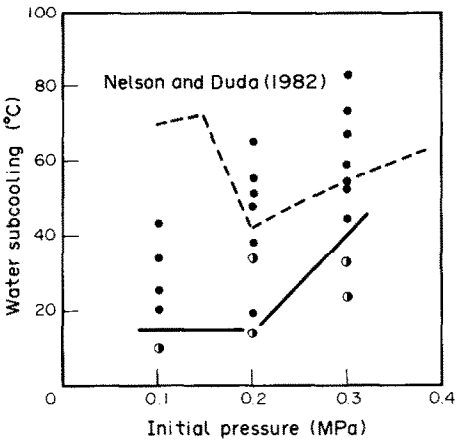

FIG. 6. Effect of water subcooling on triggering interactions at various initial pressures: $T_f = 560$–$580\,^{\circ}C$, $\Delta P = 0.41$ MPa.

Nelson and Duda results. A theoretical comparison will, however, be made, based on the vapor film collapse calculation, in Section 4.5.

4. ANALYSIS AND DISCUSSION

4.1. *Fragmentation of single tin drops*

The high-speed photographs and the debris show incomplete fragmentation of tin drops, although the initial superheat of the melts was maintained greater than $300\,^{\circ}C$. It appears that freezing of the tin drop surface becomes dominant at this temperature range and inhibits further progress of the fragmentation in the later period, giving rise to a porous shell-like debris. A similar type of debris was also obtained by Bradley and Witte [18] in the molten metal jet–water interaction experiments. The jet was found to be expanded into a popcorn appearance and solidified in that configuration when the superheating of the melt was less than $100\,^{\circ}C$.

If the surface freezing is competitive with fragmentation of fuel drops, the fragmentation time should be less than the freezing time, during which crust on the surface grows to a thickness comparable to the minimum particle size, for extensive fragmentation of fuel drops.

The crust growth is given by [19]

$$X(t) = 2\lambda(\alpha_f t)^{1/2} \tag{1}$$

where λ is given by

$$\frac{k_l\alpha_s^{1/2}\exp(-\lambda^2)}{k_s\alpha_l^{1/2} + k_l\alpha_s^{1/2}\operatorname{erf}(\lambda)} - \frac{k_f\alpha_s^{1/2}(T_f - T_m)\exp[-\lambda^2(\alpha_s/\alpha_f)]}{k_s\alpha_f^{1/2}(T_m - T_l)\operatorname{erfc}[\lambda(\alpha_s/\alpha_f)^{1/2}]} = \frac{h_{sf}\pi^{1/2}\lambda}{C_{ps}(T_m - T_l)}. \tag{2}$$

For fuel temperatures close to the melting point, the second term on the left-hand side becomes negligible. Then, the constant λ is 0.2 for water at $50\,^{\circ}C$, and a crust of thickness 0.2 mm will be developed on the surface in about 1 ms. If the cooling time scale of the thermal boundary layer on the surface is less than 1 ms, fragmentation into particles of diameters much less than 0.2 mm will not be possible.

4.2. *Empirical correlation for the fragmentation time*

The fragmentation time scale can be estimated from the time intervals between pressure peaks. The high-speed photographs (Fig. 4) show that the maximum expansion of the boundary occurs after the third collapse of the vapor/gas region, and no significant change in the boundary occurs after that. Hence, the time intervals between the first and third pressure peaks would be a good approximation of the fragmentation time scale.

The variables involved in fragmentation are t_b, fragmentation time, T_{f0}, the initial tin drop temperature, T_{l0}, the initial water temperature, ΔP, the shock pressure, D, the drop diameter, and P_0, the initial pressure. Here the same form of dimensionless time as in the hydrodynamic fragmentation is defined

$$T^+ = \frac{t_b u_c}{D}\left(\frac{\rho_l}{\rho_f}\right)^{1/2} \tag{3}$$

where u_c is the characteristic velocity for vapor film collapse, which can be expressed as [4]

$$u_c = \left(\frac{\Delta P}{\rho_l}\right)^{1/2}. \tag{4}$$

The thermal effects of coolant and fuel drops can also be taken into consideration. Since the Jakob number is an important parameter in the thermally-controlled bubble growth, which is believed to come into play in multi-step fragmentation, a similar form of a thermal Jakob number is defined for fuel and coolant as

$$Ja^+ = \frac{(1-\xi)\rho_f C_{pf}\Delta T_f'}{\rho_g h_{fg}}; \quad \Delta T_f' = T_{f0} - T_{l0} + \frac{h_{sf}}{C_{pf}} \tag{5}$$

where ξ is the fraction of heat transferred from the fuel drop which is lost to the surrounding water.

On the other hand, the thermal Weber number is defined as

$$We^+ = \frac{\rho_l X_0 u_c^2}{\sigma_f} \tag{6}$$

where X_0 is the initial film thickness, given by [20]

$$X_0 = \frac{D}{2}\left[\exp\left\{4.35\left(\frac{k_g\mu_g\Delta T_{sat}}{h_{fg}'D\rho_g\sigma}\right)^{1/4}\right\} - 1\right] \tag{7}$$

$$h_{fg}' = h_{fg} + 0.95C_{pg}(T_f - T_{sat}). \tag{8}$$

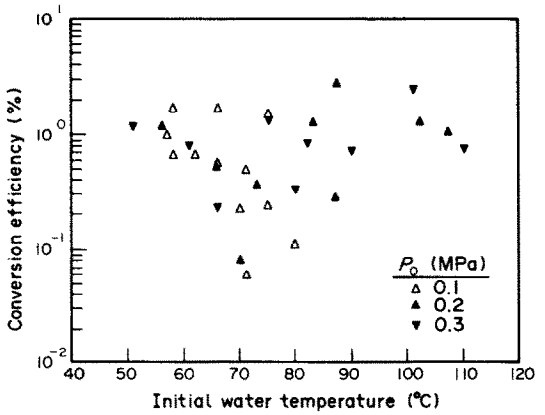

FIG. 7. Conversion efficiency vs initial water temperature at various initial pressures: $\Delta P = 0.41$ MPa, $T_f = 550$–$580\,^{\circ}C$.

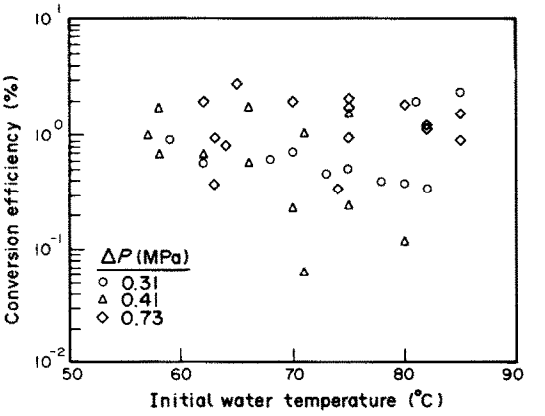

FIG. 8. Conversion efficiency vs initial water temperature at various shock pressures: $P_0 = 0.1$ MPa, $T_f = 550$–$580\,^{\circ}C$.

When these variables are correlated, based on the experimental data, in an equation of the form

$$T^+ = a Ja^{+m} We^{+n} \tag{9}$$

one obtains $a = 9.6$, $m = -0.42$, $n = -0.23$ with variances of 7.1×10^{-2}, 7.4×10^{-3}, 5.7×10^{-3} for a one-step process, and $a = 1.3$, $m = -0.3$, $n = 0.21$ with variances of 2.2×10^{-2}, 2.3×10^{-3}, 1.8×10^{-3} for a multi-step process, where ξ was taken as 0.9. For $\xi = 0.75$, only the value for a varies slightly, while the values for m and n are still the same as for $\xi = 0.9$; $a = 14.1$ with variance of 8.9×10^{-2} for a single-step process, and $a = 1.7$ with variance of 2.8×10^{-2} for a multi-step process.

4.3. *Conversion of thermal energy*

The initial calculation of the mechanical work available from a molten fuel/coolant interaction was made purely on thermodynamic grounds by Hicks and Menzies [21]. The calculation gives the thermodynamic upper limit on the potential work, which could be as much as 30% of the total thermal energy in the molten fuel. Taking into account the heat loss in this case to the surrounding water which ranges from 75 to 90% of the heat transfer from the fuel surface [22, 23], the conversion efficiency is significantly reduced. Experimental values of the conversion efficiency are usually much less than 10% [24–26].

We take the mechanical work done by the water column above the interaction region as the main output from the thermal energy release process. If the compression of the water below the interaction region is negligible, the kinetic energy of the water column can be estimated by the pressure impulse, which is calculated from the measured pressure history in water and the gas phase above the water.

The calculated conversion efficiencies of the kinetic energy are shown in Figs. 7 and 8. Here, the upper limit of the integration time for the maximum pressure impulse was taken as the time for the third pressure peak, because the high-speed photographs (Fig. 4) show a maximum expansion of the boundary immediately after the third collapse of the vapor/gas region. It is seen that the wide scatter in calculated efficiency makes it difficult to separate parametric effects. In general, the efficiencies are in the range of 0.1–1%.

4.4. *Heat transfer during fuel–coolant interactions*

Duffey *et al.* [22] measured the transient heat transfer and vapor generation rates in water under conditions of acoustic and high-pressure loading. They found that near the nucleate boiling region the peak flux was 5–10×10^7 W m^{-2} and only about 10% of the thermal energy contributes to generate a vapor phase. Inoue and Bankoff [11] also measured the peak heat flux in Freon-113 in a study of destabilization of film boiling due to arrival of a pressure shock, and reported a value of the order of 10^6 W m^{-2}.

Since the heat transfer rate in film boiling is much less than that in nucleate boiling, a sudden increase in the heat transfer rate is expected when the vapor bubble collapses. Hence, it is very difficult to estimate exactly the heat transfer rate during fragmentation. Instead, the average heat transfer rate during fuel–coolant interaction can be estimated as

$$q = \frac{\Delta H_f}{t_\infty}; \quad \Delta H_f = m_f [C_{pf}(T_f - T_l) + h_{sf}] \tag{10}$$

where the final temperature of the tin drop was assumed to be equal to the initial water temperature and t_∞ is the total elapsed time for the vapor to leave the drop as it cools. Since the initial thermal energy of the tin drops is in the range of 150–200 J and t_∞ is about 100 ms from the high-speed photographs, the average heat transfer of 1.5–2×10^3 W is obtained. For unfragmented single tin drops of diameter 1 cm, the heat transfer area is about 3×10^{-4} m^2. If surface area increases by a factor of 10 after fragmentation, the average heat flux during the interaction becomes 5–6.7×10^2 kW m^{-2}. In the Nelson and Duda experiment [9], the total elapsed time for complete fragmen-

tation was less than 10 ms. Since the initial temperature of fuel (iron oxide) was about 2000 °C and the initial water temperature about 20 °C, the average heat transfer rate becomes at least 10^4 W, using a specific heat of 800 $J\,kg^{-1}\,°C^{-1}$.

In order to scale the heat transfer time constant, during which most of the thermal energy is released, a simple calculation is performed.

If the diameter of the fuel particles during fragmentation is given by

$$-D_f = D_{f0}\exp(-t/\tau_b) \tag{11}$$

or

$$A_f = A_{f0}\exp(+t/\tau_b) \tag{12}$$

where τ_b is the fragmentation time constant and A_f is the total heat transfer area. Here the assumption is made that the fuel drops are fragmented into smaller particles with a uniform size each time. Then the energy balance for the fuel drops becomes

$$-m_f C_{pf}\frac{dT_f}{dt} = h_f A_f (T_f - T_l) \tag{13}$$

where m_f is the total mass of fuel, h_f is the average heat transfer coefficient and A_f is the total heat transfer area.

From equations (12) and (13), the change of fuel temperature is given by

$$\ln\left(\frac{T_f - T_l}{T_{f0} - T_l}\right) = -\left(\frac{h_f A_{f0}\tau_b}{m_f C_{pf}}\right)[\exp(t/\tau_b) - 1]. \tag{14}$$

Since fragmentation ceases as the fuel temperature decreases to the melting point, heat transfer without area enhancement will ensue after the time t_m, which is given by

$$\frac{t_m}{\tau_b} = \ln\left[1 - \left(\frac{m_f C_{pf}}{h_f A_{f0}\tau_b}\right)\ln\left(\frac{T_m - T_l}{T_{f0} - T_l}\right)\right]. \tag{15}$$

For the tin–water system, this time t_m is 3 ms if a water temperature of 50 °C, tin temperature of 600 °C and fragmentation time of 1 ms are assumed. For a fragmentation time of 0.1 ms, t_m is 0.8 ms. Here the film boiling heat transfer coefficient in a saturated liquid is taken from Bromley [27].

The heat transfer rate is then given by

$$\frac{q}{q_0} = \exp\left\{\frac{t}{\tau_b} - \left(\frac{h_f A_{f0}\tau_b}{m_f C_{pf}}\right)[\exp(t/\tau_b) - 1]\right\}. \tag{16}$$

Figure 9 shows the dimensionless heat transfer rate as a function of the fragmentation time. It is seen that the fragmentation time should be of the order of 1 ms for explosive interactions. Otherwise, area enhancement will be overwhelmed by the cooling of fuel drops. When the fragmentation time is 10 ms, the heat transfer rate shows a maximum and decreases sharply.

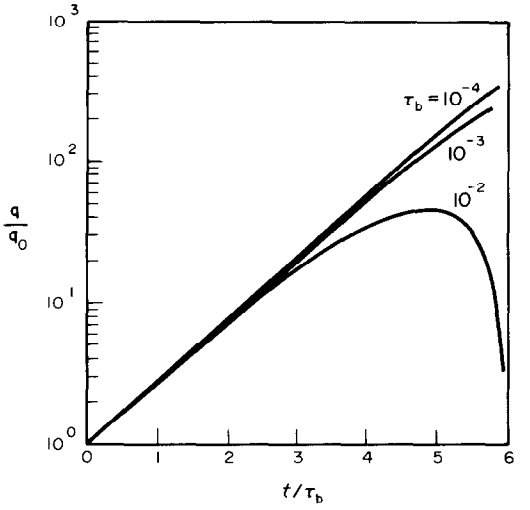

FIG. 9. Effect of the breakup time on heat transfer rate.

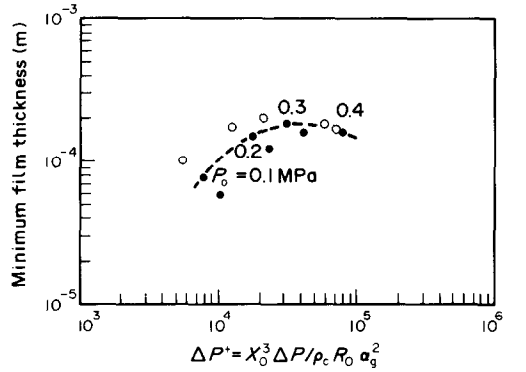

FIG. 10. Minimum film thickness vs dimensionless threshold shock pressure.

4.5. *Vapor film collapse and initiation of fuel–coolant interactions*

As shown in Fig. 5, the required trigger pressure for strong interactions decreases at initial pressures of less than 0.2 MPa in the Nelson and Duda experiment [17], while the present results show a constant trigger pressure at initial pressures of less than 0.3 MPa. This may be related to the vapor film collapse as well as the difference in the triggering mechanism; that is, a pressure shock vs a pressure pulse.

In order to examine the role of initial vapor film collapse in triggering fuel–coolant interactions, the simplified model for destabilization of film boiling [28] was recalculated for the present experimental conditions, and also the Nelson and Duda conditions.

Figure 10 shows the minimum film thickness vs dimensionless shock pressure for the present experiment. The ambient pressure was varied according to a first-order response of the form

$$P(t) - P_0 = (P_f - P_0)[1 - \exp(-t/\tau_p)] \tag{17}$$

with the time constant $\tau_p = 0.5$ ms. The minimum film thickness, X^*, at the threshold shock pressure is

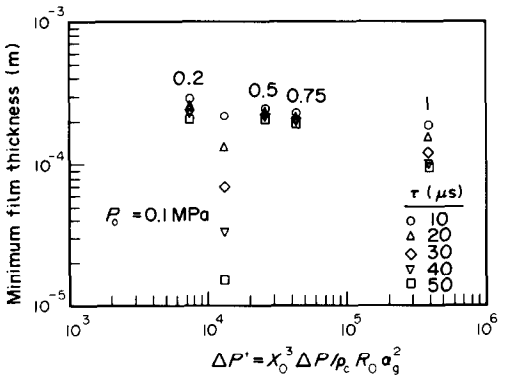

FIG. 11. Effect of the duration time of the pressure pulse on the minimum film thickness at the threshold conditions for the Nelson and Duda results.

shown by a broken line. It is seen that as the initial pressure increases at constant ΔP, ΔP^+ decreases, and X^* increases. At the initial pressure of 0.3 MPa, the increase in the shock pressure does not make much difference in the minimum film thickness. The increased vapor density at higher initial pressure comes into play to impede collapse of the vapor film.

Since it was found that the reproducibility of the trigger pressure pulses using an exploding wire is not very good [29], the effect of the duration time was examined for the Nelson and Duda results. Here the pressure pulse was approximated as a square wave with an amplitude ΔP and a duration time in the range of 10 μs. Figure 11 shows that the minimum film thickness is very sensitive to the duration time at atmospheric pressure, while the minimum film thickness varies little at initial pressures greater than 0.2 MPa. As the duration time decreases, the minimum film thickness approaches the values at higher initial pressures. If the fuel–coolant interaction can be initiated as soon as the vapor film thickness reduces to a certain critical value, for example 2×10^{-4} m in the Nelson and Duda experiment, strong interactions would be triggered by a pressure pulse as low as 0.1 MPa with a duration time of 20 μs. Thus, it may be concluded that, since the behavior of the vapor film collapse is very much dependent upon the duration time of the pressure pulse, especially at 0.1 MPa, a more careful examination should be performed of the triggering phenomenon at low initial pressures.

5. CONCLUSIONS

(1) Thermal interactions of a tin drop with water have been studied with a dropping-contact mode in a shock tube geometry. The interaction was triggered by collapsing the initial vapor/gas bubble with a pressure shock, giving rise to a hollow, porous, shell-like debris. It appears that freezing of the drop surface suppresses the fragmentation process and inhibits complete fragmentation of tin drops into fine particles. Hence, only the intermediate stage of the fragmentation process was observed. The debris indicates that violent boiling, or homogeneous nucleation, of penetrated water seems to be a dominant mechanism for fragmentation of tin drops. The porous state of the shell also indicates strong turbulence and mixing in this region. Flows of 10 m s^{-1} past 100 μm bubbles will easily satisfy a turbulent Reynolds number criterion as high as 10^3. If the characteristic length is taken to be the thickness of the foamed layer, the required velocities are at least an order of magnitude lower. However, further studies on this area should be performed to develop a more deterministic model.

(2) A decrease in the threshold trigger pressure at initial pressures less than 0.2 MPa, as observed in the Nelson and Duda experiment [17], was not found in the present experiment. This may be related to a more stable vapor film, owing to higher iron oxide temperatures. Hence, a stronger trigger pulse was necessary in the Nelson and Duda experiment. Besides, the triggers were quite different; a pressure shock, instead of a pressure pulse, was used in the present experiment. Hence, the ambient pressure remained at a higher pressure than the initial pressure during the interaction, while the ambient pressure returned nearly instantaneously to the initial pressure in the Nelson and Duda experiment. Since the reproducibility of the trigger pulse using an exploding wire is not very good, the effect of the duration time for the trigger pulse on the vapor film collapse was examined, based on a simplified model for destabilization of film boiling. It was found that the minimum film thickness at the cutoff conditions is strongly dependent upon the duration time, which varied between 10 and 50 μs, at atmospheric pressure, but not at higher initial pressures greater than 0.2 MPa. Therefore, a more careful examination is needed of the 'easier triggering' range.

(3) The average heat transfer rate during the interaction was found to be in the range 1–10 kW. When a surface area increase by a factor of 10 is assumed for a drop of initial diameter 1 cm, the average heat flux was at least one order of magnitude less than the peak heat flux measured by Duffey *et al.* (5–10 kW cm^{-2}). Furthermore, if an exponential increase in the surface area is assumed during the interaction, it was found that the fragmentation time should be of the order of 1 ms for strong interactions. Otherwise, the area increase will be overwhelmed by cooling of fuel drops, resulting in early onset of freezing.

(4) If fragmentation is a multi-step process, as observed in the Nelson and Duda experiment, the fragmentation time scale may be approximated as the time intervals between the first and third pressure peaks. The dimensionless breakup time was correlated, in terms of a modified Jakob number, and a thermal Weber number, in an equation of the form

$$T^+ = a Ja^{+m} We^{+n}$$

where $m = -0.3$ and $n = 0.21$ were obtained, while a varies in the range 1.3–1.7, depending on the heat loss to the surrounding water.

(5) The conversion efficiency of thermal energy to mechanical energy of the water column above the interaction region was also calculated, based on the incompressible liquid momentum equation. Even though wide scatter in the calculated conversion efficiencies makes it difficult to separate parametric effects, the efficiencies are in the range of 0.1–1%, which is much less than the Hicks and Menzies values.

Acknowledgement—This work was supported by the Department of Energy (DE-AC02-76ET37210), administered through the Division of Educational Programs, Argonne National Laboratory.

REFERENCES

1. M. L. Corradini and D. V. Swenson, Probability of containment failure due to steam explosions following a postulated core meltdown in an LWR, NUREG/CR-2214 SAND80-2132 R3, Sandia Nat. Labs (1981).
2. T. P. Fishlock, Calculations on propagating vapor explosions for the aluminum/water and UO_2/sodium systems, *Proc. 4th CSNI Specialist Mtg. on FCI*, Bournemouth, U.K. (1979).
3. D. Swift and L. Baker, Experimental studies of high-temperature interaction of fuel and cladding materials and liquid sodium, ANL-7120, Argonne Nat. Lab. (1965).
4. D. J. Buchanan, A model for fuel–coolant interactions, *J. Phys. D: Appl. Phys.* **7**, 1441–1457 (1974)
5. F. E. Brauer, N. W. Green and R. B. Mesler, Metal/water explosions, *Nucl. Sci. Engng* **31**, 551–554 (1968).
6. S. J. Board, C. L. Farmer and D. H. Poole, Fragmentation in thermal explosions, *Int. J. Heat Mass Transfer* **17**, 331–339 (1974).
7. B. O. Wey, R. W. Hall, S. J. Board and M. Baines, Boiling fragmentation studies and their relevance to the initiation and propagation of FCIs, ICHMT Seminar, Dubrovnik (1980).
8. A. Sharon and S. G. Bankoff, Fuel–coolant interactions in a shock tube with initially-established film boiling, ANS/ENS Int. Mtg. on Fast Reactor Safety Technology, Seattle, Washington (1979).
9. L. S. Nelson and P. M. Duda, Steam-explosion experiments with single drops of iron oxide melted with a CO_2 laser, NUREG/CR-2295 SAND81-1346 R3, Sandia Nat. Labs (1981).
10. M. Anderle, G. Frohlich, M. Burger, W. Schwalbe and H. Unger, Contribution to the interpretation of Nelson's iron-oxide-droplet-experiments, CSNI/OECD Joint Interpretation Exercise on Selected Fuel–Coolant Interaction Experiments, Karlsruhe (1980).
11. A. Inoue and S. G. Bankoff, Destabilization of film boiling due to arrival of a pressure shock—Part I: Experimental, *J. Heat Transfer* **103**, 459–464 (1981).
12. T. A. Dullforce, D. J. Buchanan and R. S. Peckover, Self-triggering of small scale fuel–coolant interactions: I. Experiments, *J. Phys. D: Appl. Phys.* **9**, 1295–1303 (1976).
13. J. A. Reynolds, T. A. Dullforce, R. S. Peckover and G. J. Vaughan, Fuel–coolant interactions—some basic studies at the UKAEA Culham Laboratory, *Proc. 3rd Spec. Mtg. on Sodium/Fuel Interactions in Fast Reactors*, Tokyo, Japan (1976)
14. D. H. Cho, W. H. Gunther and D. R. Armstrong, Fragmentation of molten materials dropped into water, ANL-8155, Argonne Nat. Lab. (1974).
15. S. H. Han, Molten fuel–coolant interactions, Ph.D. Dissertation, Chemical Engineering Dept., Northwestern University, Evanston, Illinois (1984).
16. M. Ochiai and S. G. Bankoff, A local propagation theory for vapor explosions, *Proc. 3rd Spec. Mtg. on Sodium/Fuel Interaction in Fast Reactors*, Tokyo, Japan (1976).
17. L. S. Nelson and P. M. Duda, Steam explosions of molten iron oxide drops: easier initiation at small pressurizations, *Nature* **296**, 844–846 (1982).
18. R. H. Bradley and L. C. Witte, Explosive interaction of molten metals injected into water, *Nucl. Sci. Engng* **48**, 387–396 (1972).
19. H. S. Carslaw and J. C. Jaegar, *Conduction of Heat in Solids*, 2nd edn. Oxford University Press, Oxford (1959).
20. K. J. Baumeister and T. D. Hamill, Film boiling from a thin wire as an optimal boundary-value process, ASME Paper 67-HT-62, 7th Heat Transfer Conf., Seattle (1967).
21 E. P. Hicks and D. C. Menzies, Theoretical studies on the fast reactor maximum accident, ANL-7120, Argonne Nat. Lab. (1965).
22. R. B. Duffey, A. J. Clare, D. H. Poole, S. J. Board and R. S. Hall, Measurements of transient heat fluxes and vapor generation rates in water, *Int. J. Heat Mass Transfer* **16**, 1513–1525 (1973).
23. S. G. Bankoff, F. Kovarik and J. W. Yang, A model for fragmentation of molten metal oxides in contact with water, *Proc. Int. Mtg. on LWR Severe Accident Evaluation*, Cambridge (1983).
24. M. J. Bird, An experimental study of scaling in core melt/water interactions, AIChE–ASME National Heat Transfer Conference, Niagara Falls (1984).
25. D. E. Mitchell, M. L. Corradini and W. W. Tarbell, Intermediate scale steam explosion phenomena: experiments and analysis, NUREG/CR-2145 SAND81-0124 R3, Sandia Nat. Labs (1981).
26. L. W. Deitrich, Evaluation of energy conversion in TREAT Mark-II loop experiments, *Trans. Am. Nucl. Soc.* **14**, 278 (1971).
27. L. A. Bromley, Heat transfer in stable film boiling, *Chem. Engng Prog.* **46**, 221 (1950).
28. A. Inoue, A. Ganguli and S. G. Bankoff, Destabilization of film boiling due to arrival of a pressure shock. Part II: analytical, *J. Heat Transfer* **103**, 465—471 (1981).
29. M. L. Corradini, Private communication (1984).

INTERACTIONS D'UNE GOUTTE D'ETAIN FONDU AVEC L'EAU, DECLENCHEES PAR UN CHOC BASSE-PRESSION

Résumé—Les interactions thermiques d'une goutte d'étain fondu avec de l'eau sont étudiées avec un mode de contact obtenu dans une géométrie de tube à choc. L'interaction est déclenchée en faisant disparaître la bulle initiale vapeur/gaz par un choc à basse pression ($< 0{,}8$ MPa). Le débris creux, poreux en forme de coquille montre que la violente ébullition (ou la nucléation homogène) d'eau qui a pénétré, suivie par un mélange turbulent, peut être un mécanisme dominant pour la fragmentation des gouttes d'étain. On obtient une formule empirique pour l'échelle de temps de fragmentation. Le flux moyen de chaleur transféré pendant l'interaction est compris entre 1 et 10 kW. Le rendement de la conversion de l'énergie thermique en énergie mécanique de la colonne d'equ au-dessus de la goutte d'étain est situé dans le domaine 0,1–1,0%.

THERMISCHE WECHSELWIRKUNGEN EINES GESCHMOLZENEN ZINNTROPFENS MIT WASSER, AUSGELÖST DURCH EINEN UNTERDRUCKSTOSS

Zusammenfassung—Die thermischen Wechselwirkungen eines geschmolzenen Zinntropfens mit Wasser wurden in einem Stoßrohr untersucht. Die Wechselwirkung wurde durch den Zusammenbruch einer anfänglich vorhandenen Dampf-/Gasblase infolge eines Druck-Stoßes ausgelöst ($<0{,}8$ MPa). Das hohle, poröse, schalenförmige Bruchstück läßt vermuten, daß heftiges Sieden—oder homogene Keimbildung—in Wasser, gefolgt von turbulenter Vermischung, der Hauptmechanismus bei der Zertrümmerung von Zinntropfen ist. Für den Zeitmaßstab der Zertrümmerung wurde eine empirische Korrelation gefunden. Der mittlere Wärmeaustausch während der Wechselwirkungen bewegt sich in einem Bereich von 1 bis 10 kW. Der Konversionsfaktor von thermischer in mechanische Energie der Wassersäule über dem Zinntropfen beträgt 0,1–1,0%.

ТЕПЛОВОЕ ВЗАИМОДЕЙСТВИЕ КАПЛИ РАСПЛАВЛЕННОГО ОЛОВА С ВОДОЙ ПРИ ПРОХОЖДЕНИИ УДАРНОЙ ВОЛНЫ МАЛОЙ ИНТЕНСИВНОСТИ

Аннотация—Тепловое взаимодействие капли расплавленного олова с водой исследовалось на установке типа ударной трубы. Взаимодействие инициировалось при разрушении паро-газового пузырька ударной волной малой интенсивности ($<0{,}8$ МПа). Анализ пустотелых, пористых, скорлупообразных остатков показывает, что наиболее вероятным механизмом разрушения капель олова является бурное кипение проникающей в поверхность капли воды или однородное образование пузырьков с последующим турбулентным перемешиванием. Получено эмпирическое соотношение для определения шкалы времени разрушения пузырьков. Найдено, что значение средней мощности теплового потока лежит в пределах 1–10 кВт. Показано, что доля преобразования тепловой энергии в механическую энергию водяного столба над каплей олова составляет 0,1–1,0%.